CALPHAD: Computer Coupling of Phase Diagrams and Thermochemistry xx (xxxx) xxxx–xxxx

Contents lists available at ScienceDirect

CALPHAD: Computer Coupling of Phase Diagrams and Thermochemistry

journal homepage: www.elsevier.com/locate/calphad

Experimental study and thermodynamic modelling of the B-Fe-Mn ternary system

Peter Repovský[a], Viera Homolová[a,*], Lucia Čiripová[a], Aleš Kroupa[b], Adéla Zemanová[b]

[a] Institute of Materials Research, Slovak Academy of Sciences, Watsonova 47, 040 01 Košice, Slovakia
[b] Institute of Physics of Materials, Academy of Sciences of the Czech Republic, Žižkova 22, 616 62 Brno, Czech Republic

ARTICLE INFO

Key words:
Thermodynamic modelling
Phase diagram
Borides
CALPHAD-method

ABSTRACT

This work is focused on an experimental study of phase equilibria in the B-Fe-Mn ternary system combined with a CALPHAD theoretical analysis with the aim of creating a reliable theoretical thermodynamic dataset for calculation of the phase diagram of the ternary system. Boron is modelled as an interstitial element in all solid solutions of Fe and Mn. In the experimental study, B-Mn-Fe alloys were prepared and heat-treated at 873 K for 90 days/2160 h and at 1223 K for 60 days/1440 h. Following heat treatment, the phase equilibria and composition of the coexisting phases were determined using scanning electron microscopy and X-ray diffraction analysis. The experimental results obtained, together with experimental results collected from the literature, were used in the optimization of the thermodynamic parameters by using the CALPHAD method. The result of this work is an optimized thermodynamic dataset for the B-Fe-Mn ternary system allowing the phase diagram and thermodynamic properties to be calculated.

1. Introduction

The B-Fe-Mn system is an important subsystem in various classes of boron containing steels, for example in steels for the energy industry [1], and in MnB steels [2–4], which have excellent mechanical properties and are used in the automotive industry. This system is also important for materials having excellent magnetic properties [5,6], cast irons [7,8] and wear resistant materials [9]. Boron and manganese are also useful alloying elements that can improve the strength of many advanced metallic (e.g., Al, Cu, Fe and Ni-based) materials.

This system has been studied by only a few authors. Kuzma [10] investigated experimentally the phase constitution of the B-Fe-Mn system at 1073 K (800 °C). The melting temperatures and primary phases of B-Fe-Mn alloys were studied by Gianoglio and Pradelli [11]. Thermodynamic properties, such as partial enthalpies of mixing of the liquid phase, were measured by Witusiewicz [12]. This system was studied theoretically by Miettinen [13]. However, only the Fe-rich corner was modelled, with boron considered as a substitutional element in iron and manganese solid solutions.

The present work is focused on modelling the ternary B-Fe-Mn system by the CALPHAD method using new experimental results in conjunction with those outlined above. In the present work, boron is modelled as an interstitial element in all solid solutions in the system.

2. Experimental procedure

Model alloys were prepared from high purity powders or granules (Fe – 99.98% or 99.96%; Mn – 99.98% or 99.95%, B – 99.95%) that were mixed and pressed into cylindrical pellets at a pressure of 700 MPa. The pellets were then melted in an argon arc furnace to produce the alloys. The solidified alloys (5–7 g) were re-melted several times in order to achieve good homogeneity. This process resulted in samples having a weight loss in the region of 0.015–0.077 g. Therefore, the true chemical compositions of the alloys were determined following the arc-melting process using Atomic Absorption Spectroscopy (Table 1). The alloys were then sealed in evacuated silica glass tubes and annealed under the following conditions: 2160 h at 873 K and 1440 h at 1223 K. Following annealing, the samples were quenched into cold water.

The annealed material was studied using a JEOL JSM-7000F Scanning Electron Microscope equipped with “Thermal FEG” and an INCA EDX analyzer. The EDX analyzer enabled quantitative analysis for elements above and including atomic number 5 (boron). The phase composition of the alloys was determined by X-ray diffraction (Philips X´Pert Pro).

* Corresponding author.

http://dx.doi.org/10.1016/j.calphad.2016.10.002
Received 19 August 2016; Received in revised form 6 October 2016; Accepted 8 October 2016
Available online xxxx
0364-5916/

Table 1
Chemical composition of model alloys and their phase composition after annealing.

Alloy	Composition [at%]	Phase composition 873 K/1223 K
1	30Fe-7B-63Mn	M_2B+FCC / M_2B+FCC
2	82Fe-5B-13Mn	M_2B+FCC / M_2B+FCC
3	82Fe-9B-9Mn	M_2B+BCC / M_2B+FCC
4	22Fe-39B-39Mn	MB+M_2B / MB+M_2B
5	51Fe-39B-10Mn	MB+M_2B / MB+M_2B
6	10Fe-52B-38Mn	Mn_3B_4+MB / Mn_3B_4+MB
7	32Fe-52B-16Mn	MB+Mn_3B_4 / MB+Mn_3B_4
8	41Fe-56B-3Mn	MB+B / MB+B
9	6Fe-24B-70Mn	M_2B+CBCC / M_2B+CUB
10	27Fe-24B-50Mn	M_2B+FCC / M_2B+FCC
11	33Fe-30B-37Mn	M_2B+FCC / M_2B+FCC
12	47Fe-25B-28Mn	M_2B+BCC / M_2B+FCC
13	50Fe-32B-18Mn	M_2B+BCC / M_2B+FCC
14	21Fe-57B-22Mn	Mn_3B_4+MB / Mn_3B_4+MB
15	19Fe-57B-24Mn	MB+MnB_4+Mn_3B_4 / MB+MnB_4+Mn_3B_4
16	10Fe-80B-10Mn	MB+MnB_4+B / MB+MnB_4+B
17	13Fe-78B-9Mn	MB+MnB_4+B / MB+MnB_4+B
18	37Fe-47B-16Mn	MB+M_2B / MB+M_2B

3. Thermodynamic model

3.1. Thermodynamic models for solid solutions and liquid

The sublattice model developed by Hillert and Staffansson [14] was used in the present work to describe the Gibbs energy of the individual phases. Boron was considered as an interstitial element in the B-Fe-Mn system, similarly as in the Fe-B-V system in the work of Homolova [15]. According to Guo and Kelly [16], elements such as Cr, Mo and V increase the solubility of boron in iron solutions. This is because their atomic diameters are larger than that of iron, and on forming substitutional solid solutions, there is a resulting expansion in the size of interstitial position making the interstitial dissolution of boron easier. Hence, in this work boron is considered as an interstitial element in iron solid solutions.

The Gibbs energies of the BCC_A2 (δMn), FCC_A1 (γMn), CBCC_A12 (αMn) and CUB_A13 (βMn) phases in the B-Fe-Mn system are described using the two-sublattice model. Metallic elements occupy the first sublattice, and vacancy and boron occupy the second (interstitial) sublattice. The Gibbs energy for the two sublattice model $(Fe, Mn)_a\ (B, Va)_c$ can be expressed as:

$$G_{SS}=\sum_i y_i(y_B G^0_{i:B}+y_{Va}G^0_{i:Va})+aRT\sum_i y_i ln y_i+cRT(y_B ln y_B+y_{Va}ln y_{Va}) + y_{Mn}y_{Fe}(y_B L_{Mn,Fe:B}+y_{Va}L_{Mn,Fe:Va})+y_B y_{Va}\sum_i y_i L_{i:B,Va}+G_{mag.} \quad (1)$$

$i=Fe,\ Mn$

In Eq. (1), y represents the site fraction of component i in the relevant sublattice. Symbols a and c are stoichiometric coefficients of each sublattice (for BCC: a=1 and c=3, for FCC, CBCC and CUB: a=c=1). $G^0_{i:Va}$ is the Gibbs energy of pure element i in the phase and $G^0_{i:B}$ is the Gibbs energy of a hypothetical non-magnetic boride, where element i occupies the first sublattice and all the interstitial positions are occupied by boron.

All values of G are given relative to the Standard Element Reference state (SER) that is defined as the stable state of the element under standard conditions (298.15 K and 10^5 Pa). Interaction parameters L are expressed by a Redlich-Kister polynomial [17]:

$$L_{i,j:k}=\sum_{v=0}^{n} L^v_{i,j:k}(y_i-y_j)^v \quad (2)$$

The interaction parameters $L_{i:k,m}$ and $L_{i,j:k,m}$ (where $i, j = Fe, Mn$; k, $m = B, Va$) are defined analogically.

The temperature dependence of the L^v parameter is expressed as follows:

$$L^v_{i,j:k,m}=A+BT \quad (3)$$

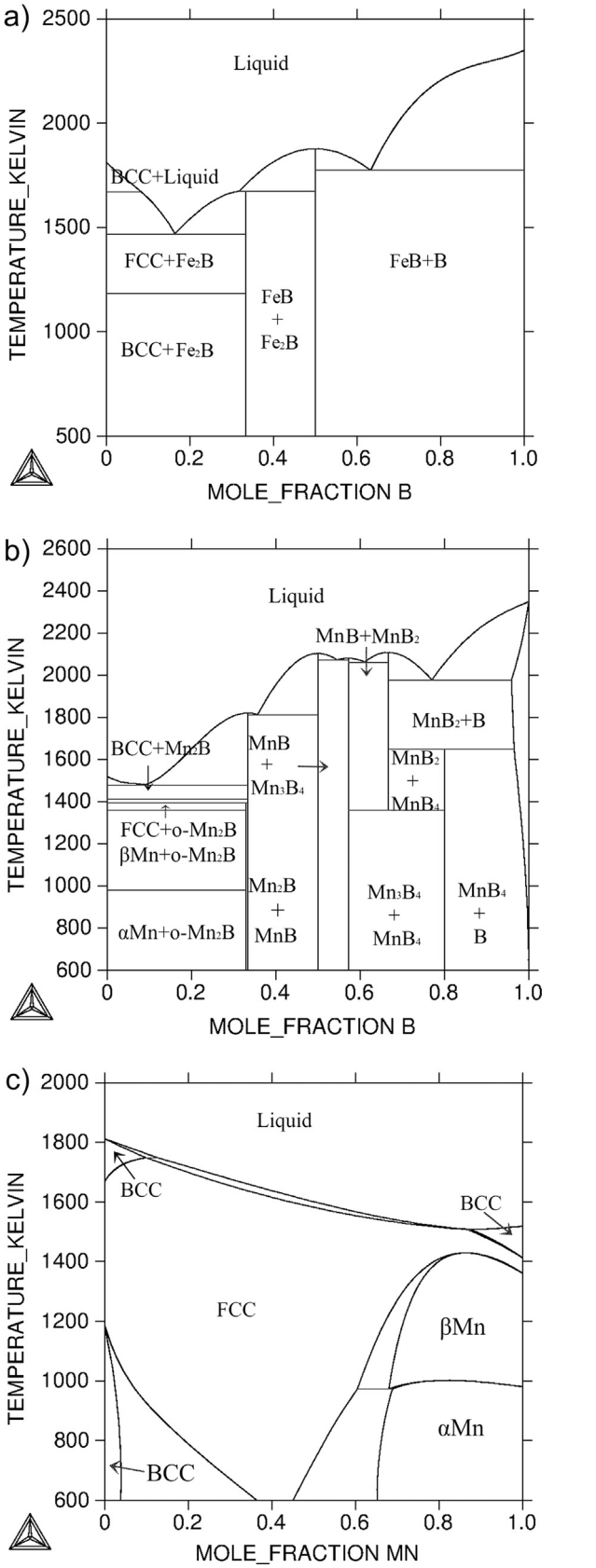

Fig. 1. Calculated binary phase diagrams: (a) Fe-B; (b) Mn-B; (c) Fe-Mn.

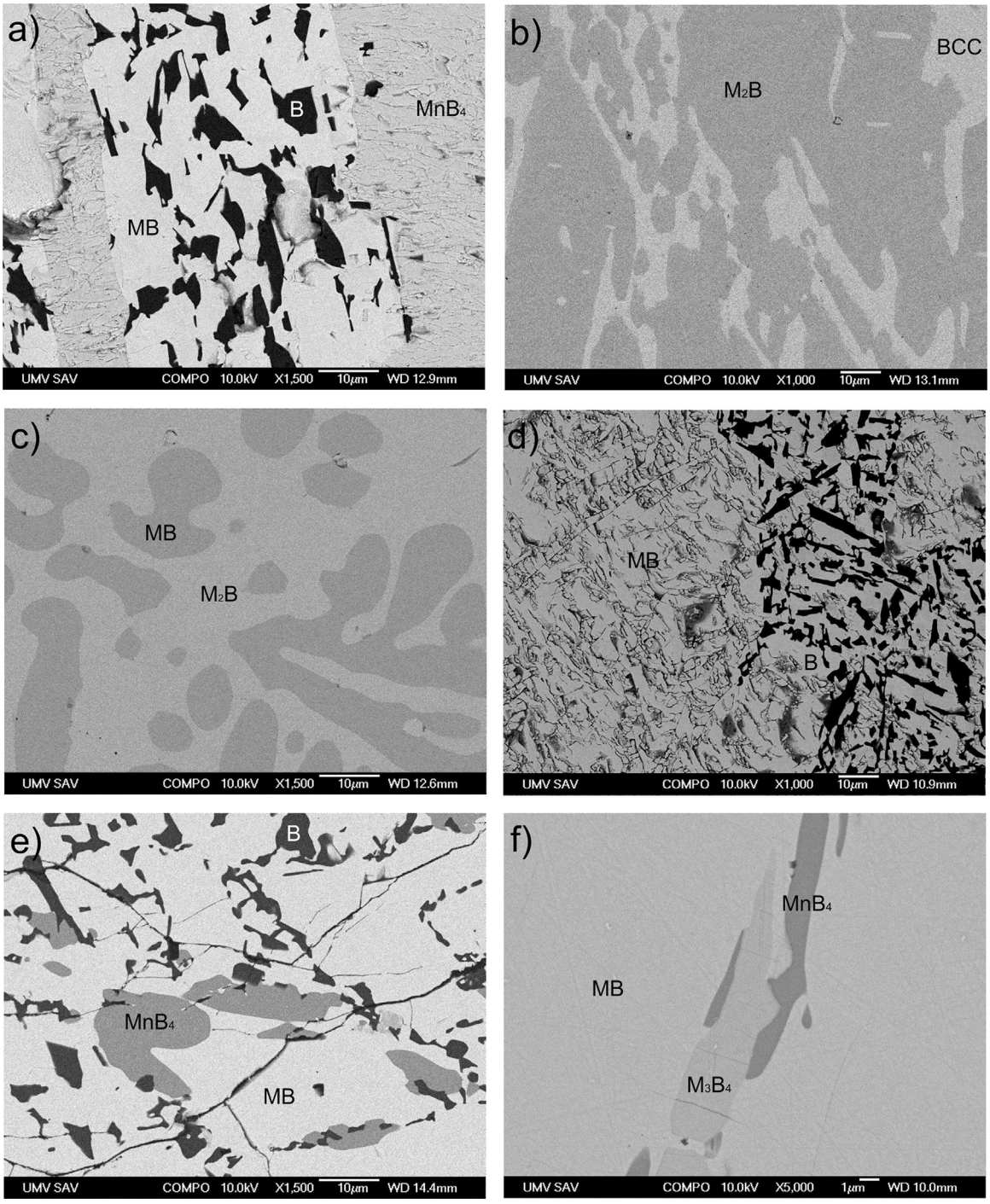

Fig. 2. Microstructure of the B-Fe-Mn alloys after annealing at 873 K: (a) alloy 16; (b) alloy 13; (c) alloy 18; and at 1223 K: (d) alloy 8; (e) alloy 17; (f) alloy 15.

G_{mag} in Eq. (1) is the magnetic contribution to the Gibbs energy. Its value is calculated according to the model of Hillert and Jarl [18].

The liquid phase is described by single sublattice. Its Gibbs energy is described as follows:

$$G_{Liquid}=\sum_i x_i G_i^0+RT\sum_i x_i ln x_i+\sum_{i,j} x_i x_j L_{i,j}+\sum_{i,j,k} x_i x_j x_k L_{i,j,k} \quad (4)$$

$i, j, k = Fe, Mn, B$

The β-rhombohedral B phase (βB) is modelled using random mixing on one sublattice.

3.2. Thermodynamic model for borides

All borides are described as stoichiometric phases with two sublattices $(Fe, Mn)_a(B)_c$. The Gibbs energy is given as follows:

$$G_{Borid}=\sum_i y_i y_B G_{i:B}^0+aRT\sum_i y_i ln y_i+cRT y_B ln y_B+y_{Mn} y_{Fe} y_B L_{Mn,Fe:B} \quad (5)$$

$i=Fe,\ Mn$

Thermo-Calc software was used for all calculations in this work [19]. Thermodynamic parameters for binary Fe-B, Mn-B, Fe-Mn systems were taken from the literature [20–22] and data for the pure elements were taken from Dinsdale [23]. Binary phase diagrams calculated using these data are shown in Fig. 1.

Table 2
Experimentally determined composition of borides, x- the phase was not predicted to be in the equilibrium in the alloy and also not found experimentally.

Alloy	Fe and Mn in M_2B [at%]		Fe and Mn in MB [at%]		Fe in Mn_3B_4 [at%]		Fe in MnB_4 [at%]	
	873 K	1223 K	873 K	1223 K	873 K	1223 K	873 K	1223 K
1	15Fe,51Mn	16Fe,50Mn	x		x		x	
2	50Fe, 16Mn	53Fe,15Mn	x		x		x	
3	56Fe,10Mn	56Fe,11Mn	x		x		x	
4	28Fe,42Mn	27Fe,43Mn	19Fe,30Mn	15Fe,35Mn	x		x	
5	57Fe,10Mn	58Fe,9Mn	41Fe,9Mn	40Fe,10Mn	x		x	
6	x		10Fe40Mn	14Fe36Mn	5	8	x	
7	x		36Fe14Mn	36Fe14Mn	5	9	x	
8	x		46Fe,3.5Mn	46Fe,4Mn	x		x	
9	10Fe,56Mn	10Fe,56Mn	x		x		x	
10	17Fe,48Mn	18Fe,48Mn	x		x		x	
11	30Fe,36Mn	29Fe,37Mn	x		x		x	
12	38Fe,27Mn	39Fe27Mn	x		x		x	
13	47Fe,19Mn	47Fe,19Mn	x		x		x	
14	x		37Fe,13Mn	37Fe13Mn	6	10	x	
15	x		35Fe,15Mn	35Fe,15Mn	6	11	3	5
16	x		36Fe,14Mn	36Fe,14Mn	x		4	7
17	x		37Fe,13Mn	36Fe,14Mn	x		4	7
18	50Fe,17Mn	48Fe,18Mn	29Fe,22Mn	27Fe,19Mn	x		x	

Table 3
List of crystallographic data of the phases in the binary systems.

Phase	Pearson symbol/space group	Lattice parameters (Å)	Ref.
δ-Mn (BCC)	*cI2/Im3m*	a=3.0806	[25]
γ-Mn (FCC)	*cF4/Fm3m*	a=3.8624	[25]
β-Mn (CUB)	*cP20/P4$_1$32*	a=6.3152	[25]
α-Mn (CBCC)	*cI58/I43m*	a=8.9139	[25]
o-$Mn_2B_{0,982}$	*oF48/Fddd*	a=14.54	[25]
		b=7.291	
		c=4.208	
t-Mn_2B (M_2B)	*tI12/I4/mcm*	a=5.148	[25]
		c=4.208	
MnB (MB)	*oP8/Pnma*	a=5.56	[25]
		b=2.977	
		c=4.145	
Mn_3B_4	*oI14/Immm*	a=3.03	[25]
		b=12.86	
		c=2.96	
MnB_2	*hP3/P6/mmm*	a=3.007	[25]
		c=3.037	
MnB_4	*mC14/C2/m*	a=5.503	[25]
		b=5.369	
		c=2.949	
		β=122.71°	
β-B	*hR108/R3m*	a=10.925	[25]
		b=23.81	
α-Fe (BCC)	*cI2/Im3m*	a=2.868	[26]
γ-Fe (FCC)	*cF4/Fm3m*	a=3.647	[26]
δ-Fe (BCC)	*cI2/Im3m*	a=2.932	[26]
FeB (MB)	*oP8/Pbnm*	a=4.0587	[26]
		b=5.5032	
		c=2.9474	
Fe_2B (M_2B)	*tI12/I4/mcm*	a=5.1103	[26]
		c=4.2494	

The binary descriptions can be used to extrapolate into the ternary system. This 'prediction' gives basic knowledge of phase equilibria in the 3-component system but does not offer information relating to any possible ternary phase or solubility of a third element in any binary phase. However, this prediction allows the identification of key compositions for experimental study thus optimizing the experimental effort. By using the PARROT module of the Thermo-Calc software [19], a complete theoretical assessment of the system was undertaken on the basis of these experimental studies in conjunction with results taken from the literature [10–12].

4. Results and discussion

4.1. Experimental results

The results of the phase analysis of model alloys are shown in Table 1. Almost all of the alloys analysed exhibit two phases in equilibrium at both investigated temperatures. Three-phase equilibria were found only in alloys 15, 16, and 17 (see Table 1). Except for alloys 3, 9, 12 and 13, the phases present are the same for both of the investigated temperatures. In alloy 9, the CBCC phase stable at 873 K has changed to the CUB phase at 1223 K. Other changes occur in the phase composition of alloys 3, 12 and 13, where the phase equilibrium M_2B/(Fe, Mn)$_2$B+BCC at 873 K changes to M_2B/(Fe, Mn)$_2$B+FCC at 1223 K. Examples of the microstructures seen in the investigated alloys are presented in Fig. 2.

The solubility of the third element in the binary borides was found to be significant in all of the studied alloys. The average values are given in Table 2. High amounts of the third element were found in the phases t-Mn_2B, Fe_2B, MnB and FeB in alloys 4, 5, 18. This is to be expected as the phases t-Mn_2B and Fe_2B have the same crystallographic structure (*tI*12). A similar situation exists for the MnB and FeB phases (*oP*8), see Table 3. This suggests complete solubility between the crystallographically identical phases. Therefore, the t-Mn_2B and Fe_2B phases are labelled as a single M_2B boride, and MnB and FeB as the MB boride. These results are consistent with work of Kuzma [10]. However, the solubilities of iron in Mn_3B_4 and MnB_4 borides are higher than those found by Kuzma [10]. Iron solubilities of about 5–6 at% at 873 K and 8–11 at% at 1223 K were found for the Mn_3B_4 phase, and 3–4 at% Fe at 873 K and 5–7 at%. Fe at 1223 K were found for MnB_4. This can be explained by the shorter time of annealing (300–500 h at 1073 K) used in the work Kuzma [10] in comparison to the present work, where the annealing time was 1440 h at 1223 K and 2160 h at 873 K. It can be concluded that Kuzma's alloys [10] had not reached full equilibrium.

4.2. Theoretical results and thermodynamic modelling

All of the experimental results indicated above were used for modelling the isothermal sections of the B-Fe-Mn phase diagram by employing the CALPHAD method. The calculated isothermal section for 873 K is shown in Fig. 3a and that for 1223 K in Fig. 3b. Comparison of the experimental results with the calculations shows good agreement between the two. The calculated isothermal section for 1073 K is compared with the experimental results from Kuzma [10] in

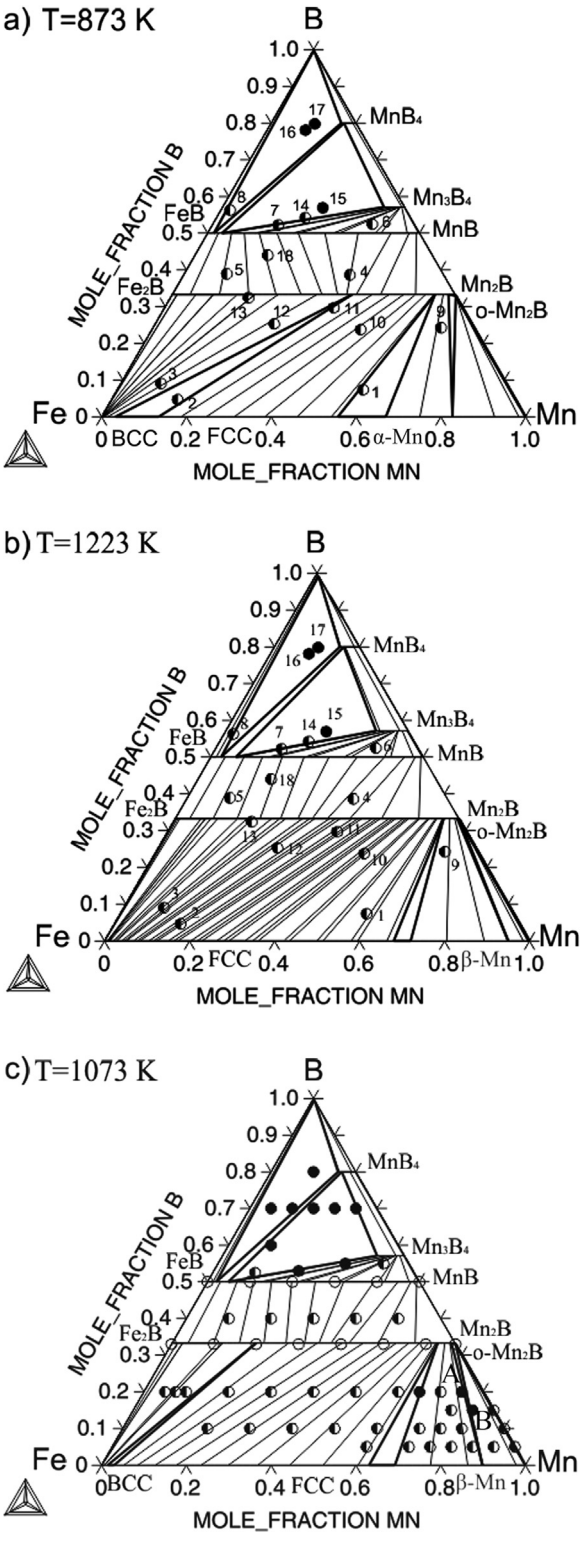

Fig. 3. Isothermal sections of the B-Fe-Mn phase diagram: (a) 873 K; (b) 1223 K; (c) 1073 K. Compositions of model alloys are marked by points, (a) and (b) from this work, (c) from [10]. Full circles represent three-phase equilibria, half-full circles represent two-phase equilibria.

Fig. 3c. The most significant difference between the calculated phase diagram and the work of Kuzma [10] is the presence of the o-Mn_2B phase in our assessment rather than the Mn_4B phase given in the earlier phase work [10]. The decision about the replacement of the Mn_4B phase is based on the work of Tergenius [24], who studied the Mn_4B phase and redefined the phase as $Mn_2B_{0,982}$. Kuzma [10] identified two alloys exhibiting the three-phase equilibrium t-Mn_2B +Mn_4B+β-Mn. These two alloys A and B are correctly located in the corresponding narrow t-Mn_2B+o-Mn_2B+β-Mn phase field, Fig. 3c in the calculated isothermal section of the phase diagram for 1073 K. Thus, despite the fact that no experimental alloys in the present work fit to the calculated phase field with the o-Mn_2B phase, it can be said that this boride is modelled in very good agreement with the experimental results from Kuzma [10].

Table 4
Calculated molar enthalpies of mixing of B-Fe-Mn.

	$(Fe_{0,75}Mn_{0,25})_{1-x}B_x$	$(Fe_{0,5}Mn_{0,5})_{1-x}B_x$	$(Fe_{0,25}Mn_{0,75})_{1-x}B_x$
x_B	$-\Delta H_{mix}$	$-\Delta H_{mix}$	$-\Delta H_{mix}$
0	3.000	4.900	4.350
0,04	6.928	8.360	7.740
0,08	10.770	11.690	11.140
0,12	13.992	14.772	14.618
0,16	17.033	17.876	18.160
0,20	19.940	20.800	21.700
0,24	22.868	23.670	28.205
0,28	25.764	25.876	28.418
0,32	28.576	28.694	31.331
0,36	31.048	31.512	33.692
0,40	33.370	34.330	36.055

The values of the molar enthalpy of mixing for liquid phase (Table 4) were calculated from the partial enthalpy of mixing published in [12] and were used in the present optimization of the thermodynamic model parameters. The calculated concentration dependence of the molar enthalpy of mixing of the liquid in the B-Fe-Mn system at 1830 K for different Fe/Mn ratios is shown in Fig. 4 together with the experimental values from Table 4. There is good agreement between calculation and experiment. Optimized parameters for the liquid phase are shown in Table 5.

The interaction parameters for the M_2B and MB phases were also optimized in this work. The optimization was based on experimentally determined solidification temperatures from the study of Pradelli and Gianoglio [11]. Again, good agreement was achieved, Fig. 5b. The optimized parameters are given in Table 5.

The dataset of optimized parameters was used to calculate the liquidus surface of the system, shown in Fig. 5. The theoretical results are compared with experimental data obtained from [11]. These experimental data points show the primary crystallization fields of individual phases at temperatures between 1473 K and 2073 K (Fig. 5b). Unfortunately, no experimental results relating to primary crystallization are known at boron contents higher than 40 at%. Therefore, experimental verification of the liquidus surface at high boron content is not possible at the present time.

The results of this work were compared with the theoretical work of Miettinen [13] which was based on experimental data from the literature only and was focused on creating a thermodynamic dataset for the iron rich region of the system. The main difference between the two assessments is in the modelling of boron in the solid solution phases. Miettinen modelled the boron as a substitutional element, while in the present work it is modelled as an interstitial element in the solid solution phases of iron and manganese. The explanation why the interstitial model was chosen here is given above. In the present paper, a slightly better agreement was achieved for the primary crystallization of the MB and M_2B phases than was found by Mietinnen [13]. Also, the higher solubility of the third element in the Mn_3B_4 and MnB_4 phases that has been observed experimentally was modelled here, contrary to the work Mietinnen.

A comparison of the theoretical modelling and experimental work shows that the developed dataset listed in Table 5 describes the phase equilibria in the system very well.

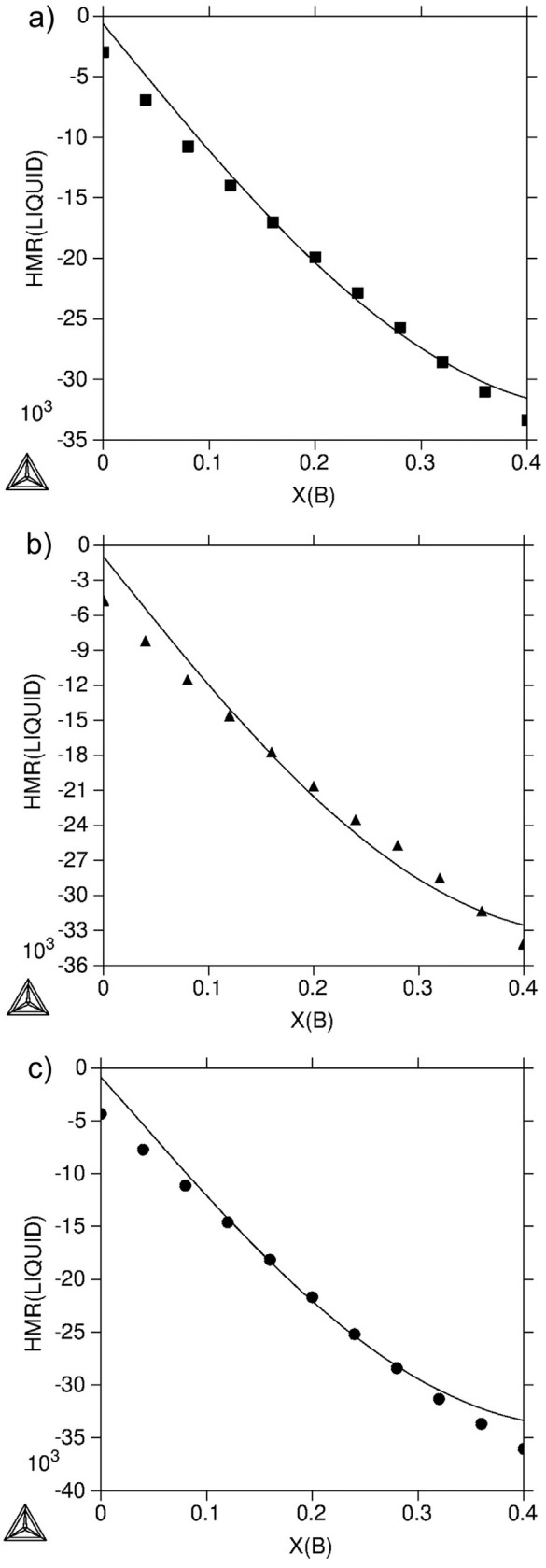

Fig. 4. Calculated molar enthalpy of mixing of liquid B-Fe-Mn alloys at 1830 K, together with experimental data: (a) Fe:Mn=3:1; (b) Fe:Mn=1:1; (c) Fe:Mn=1:3.

5. Conclusions

This work deals with the modelling of the B-Fe-Mn system by

Table 5
Thermodynamic parameters for the B-Fe-Mn system. O*- parameter optimized in this work.

Parameters	Ref.
Liquid: (B, Fe, Mn)$_1$	
${}^{o}G^{L}_{Mn}$=GMNLIQUID	[23]
${}^{o}G^{L}_{Fe}$=GFELIQUID	[23]
${}^{o}G^{L}_{B}$=GBLIQUID	[23]
${}^{o}L^{L}_{B,Fe,Mn}$=−184804.2+60*T	[O*]
${}^{1}L^{L}_{B,Fe,Mn}$=105978.9−59.96*T	[O*]
${}^{2}L^{L}_{B,Fe,Mn}$=14520.3−59.97*T	[O*]
${}^{o}L^{L}_{Fe,Mn}$=−3950+0.489*T	[22]
${}^{1}L^{L}_{Fe,Mn}$=1145	[22]
${}^{o}L^{L}_{B,Mn}$=−134141.3−15.7142*T	[21]
${}^{1}L^{L}_{B,Mn}$=32025.1−21.7659*T	[21]
${}^{2}L^{L}_{B,Mn}$=59907.4	[21]
${}^{3}L^{L}_{B,Mn}$=−8723.6	[21]
${}^{o}L^{L}_{B,Fe}$=−130243+32.152*T	[20]
${}^{1}L^{L}_{B,Fe}$=+6571	[20]
${}^{2}L^{L}_{B,Fe}$=30933	[20]
BCC: (Fe, Mn)$_1$(B, Va)$_3$	
${}^{o}G^{bcc}_{Mn:Va}$=GMNBCC	[21]
${}^{o}G^{bcc}_{Fe:Va}$=GHSERFE	[23]
${}^{o}G^{bcc}_{Mn:B}$=GMNBCC+3*GHSERB	[21]
${}^{o}G^{bcc}_{Fe:B}$=- 3000+12.832*T	[20]
${}^{o}L^{bcc}_{Fe,Mn:Va}$=− 2759+1.237*T	[22]
$\beta^{bcc}_{Fe:Va}$=2.22	[20]
$\beta^{bcc}_{Mn:Va}$=−0.27	[21]
$T^{bcc}_{C\,Fe:Va}$=1043	[20]
$T^{bcc}_{C\,Mn:Va}$=−580	[21]
$T^{bcc}_{C\,Fe,Mn:Va}$=123	[22]
FCC: (Fe, Mn)$_1$(B, Va)$_1$	
${}^{o}G^{fcc}_{Mn:Va}$=GMNFCC	[21]
${}^{o}G^{fcc}_{Fe:Va}$=GFEFCC	[20]
${}^{o}G^{fcc}_{Mn:B}$=GMNFCC+GHSERB	[21]
${}^{o}G^{fcc}_{Fe:B}$= 45496−77.534*T	[20]
${}^{o}L^{fcc}_{Fe,Mn:Va}$= −7762+3.865*T	[22]
${}^{1}L^{fcc}_{Fe,Mn:Va}$= −259	[22]
$\beta^{fcc}_{Fe:Va}$=−2.1	[22]
$\beta^{fcc}_{Mn:Va}$=−1.86	[22]
$T^{fcc}_{C\,Fe:Va}$=−201	[22]
$T^{fcc}_{C\,Mn:Va}$=−1620	[22]
CBCC: (Fe, Mn)$_1$(B, Va)$_1$	
${}^{o}G^{\alpha Mn}_{Mn:Va}$=GHSERMN	[23]
${}^{o}G^{\alpha Mn}_{Fe:Va}$=GHSERFE+4745	[23]
${}^{o}G^{\alpha Mn}_{Fe:B}$=GHSERFE+GHSERB+2000	[O*]
${}^{o}G^{\alpha Mn}_{Mn:B}$= GHSERMN+GHSERB-5000−35*T	[21]
${}^{o}L^{\alpha Mn}_{Fe,Mn:Va}$= −10184	[22]
$\beta^{\alpha Mn}_{Mn:Va}$=−0.66	[21]
$T^{\alpha Mn}_{C\,Mn:Va}$=285	[21]
CUB: (Fe, Mn)$_1$(B, Va)$_1$	
${}^{o}G^{\beta Mn}_{Mn:Va}$=GMNCUB	[23]
${}^{o}G^{\beta Mn}_{Mn:B}$=GMNCUB+GHSERB	[21]
${}^{o}G^{\beta Mn}_{Fe:Va}$=GFEBCC+3745	[20]

(continued on next page)

Table 5 *(continued)*

Parameters	Ref.
${}^{o}G_{Fe:B}^{\beta Mn}$=GFEBCC+ GHSERB+2000	[O*]
${}^{o}L_{Fe,Mn:Va}^{\beta Mn}$=−11518+2.819*T	[22]
o-$Mn_2B_{O,932}$*: (Fe, Mn)*$_2$*(B)*$_{O,932}$	
${}^{o}G_{Mn:B}^{Mn2B0,932}$=2*GHSERMN+0.982*GHSERB-94383.282−18.3989*T	[21]
${}^{o}G_{Fe:B}^{Mn2B0,932}$=2*GHSERFE+0.982* GHSERB +5000	[O*]
${}^{o}L_{Fe,Mn:B}^{Mn2B0,932}$= −15000	[O*]
M_2B*: (Fe, Mn)*$_2$*(B)*$_1$	
${}^{o}G_{Mn:B}^{M2B}$= 2*GHSERMN+GHSERB-95100−19.4406*T	[21]
${}^{o}G_{Fe:B}^{M2B}$=−96363+481.992*T-79.04999*T*LN(T)−0.007071*T^2+731991*T^{-1}	[20]
${}^{o}L_{Fe,Mn:B}^{M2B}$=−12360	[O*]
${}^{1}L_{Fe,Mn:B}^{M2B}$=+1500	[O*]
$\beta_{Fe:B}^{M2B}$=1.91	[20]
$T_{C\,Fe:B}^{M2B}$=1018	[20]
MB: (Fe, Mn)$_1$*(B)*$_1$	
${}^{o}G_{Mn:B}^{MB}$= GHSERMN+GHSERB-69600−19.999*T	[21]
${}^{o}G_{Fe:B}^{MB}$= −93615+324.299*T-50.00001*T*LN(T)−0.004999999*T^2+530000*T^{-1}	[20]
${}^{o}L_{Fe,Mn:B}^{MB}$= +4000+2*T	[O*]
${}^{1}L_{Fe,Mn:B}^{MB}$=−7000	[O*]
$\beta_{Fe:B}^{MB}$=1.03	[20]
$T_{C\,Fe:B}^{MB}$=600	[20]
Mn_3B_4*: (Fe, Mn)*$_3$*(B)*$_4$	
${}^{o}G_{Mn:B}^{Mn3B4}$=3*GHSERMN+4*GHSERB-271502−48.9328*T	[21]
${}^{o}G_{Fe:B}^{Mn3B4}$=3*GHSERFE+4*GHSERB +5000	[O*]
${}^{o}L_{Fe,Mn:B}^{Mn3B4}$=-200000	[O*]
MnB_2*: (Fe, Mn)(B)*$_2$	
${}^{o}G_{Mn:B}^{MnB2}$=GHSERMN+2*GHSERB-63300−37.668*T	[21]
${}^{o}G_{Fe:B}^{MnB2}$=GHSERFE+2* GHSERB +5000	[O*]
${}^{o}L_{Fe,Mn:B}^{MnB2}$=- 67500	[O*]
MnB_4*: (Fe, Mn)(B)*$_4$	
${}^{o}G_{Mn:B}^{MnB4}$=GHSERMN+4* GHSERB-88721.5−22.967*T	[21]
${}^{o}G_{Fe:B}^{MnB4}$=GHSERFE+4* GHSERB+5000	[O*]
${}^{o}L_{Fe,Mn:B}^{MnB4}$=-85000	[O*]
βB: (B, Mn)$_1$	
${}^{o}G_{B}^{\beta B}$=GHSERB	[23]
${}^{o}G_{Mn}^{\beta B}$=GHSERMN+40	[21]
${}^{o}L_{B,Mn}^{\beta B}$=−49500−21*T	[21]

employing the CALPHAD method using new experimental measurements presented here together with experimental data available in the literature. The results achieved can be summarized as follows:

- Boron is modelled as an interstitial element in solid solutions. All borides are modelled as stoichiometric phases with respect to boron.
- Complete solubility between the phases t-Mn_2B and Fe_2B, and between MnB and FeB was found. Based on these observations and the identical crystal structures of each pair of phases, the Fe_2B and Mn_2B phases were modelled as the M_2B/(Fe, Mn)$_2$B boride and the MnB and FeB phases were modelled as the MB/(Fe, Mn)B boride.
- The solubility of iron in the Mn_3B_4 and MnB_4 phases was determined. Its value was 5–6 at% at 873 K and 8–11 at% at 1223 K for the Mn_3B_4 phase, and 3–4 at% at 873 K and 5–7 at% at 1223 K for MnB_4 phase.
- The main result of this work is an optimized thermodynamic dataset that is suitable for thermodynamic calculations for the B-Fe-Mn ternary system. All calculations produced by the optimized dataset are in very good agreement with the literature and the new experimental results presented here.

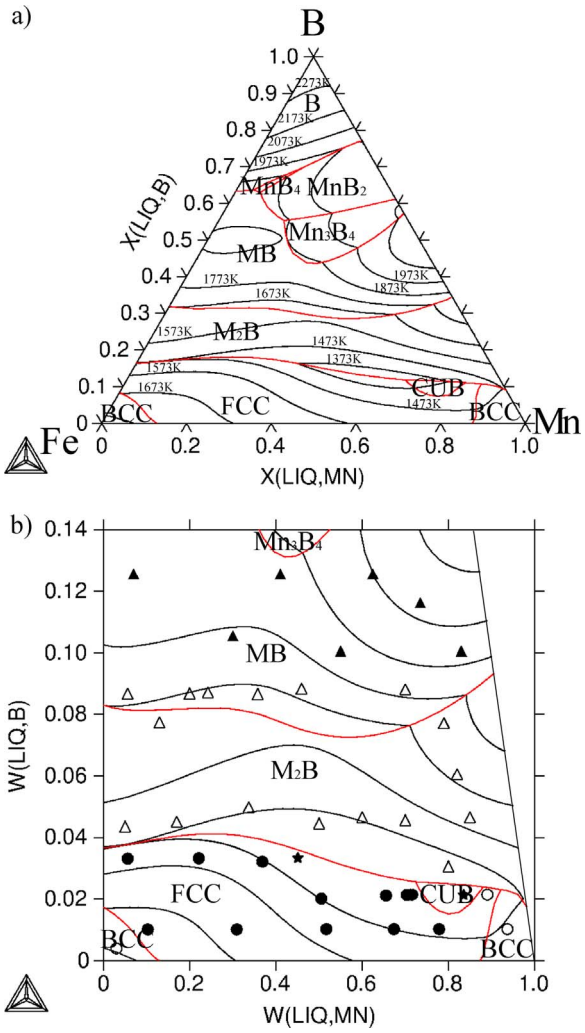

Fig. 5. (a) Calculated liquidus surface (b) detail of calculated liquidus surface for low boron content compared with experimental points.

Acknowledgements

The present work was supported by Slovak Grant Agency (VEGA) under the project No. 2/0153/15, by the Czech Science Foundation under the project No. 14–15576S and by bilateral project SAV-AVČR 15-11.

References

[1] L. Falat, V. Homolová, J. Kepič, M. Svoboda, A. Výrostková, Microstructure and properties degradation of P/T 91, 92 steels weldments in creep conditions, J. Min. Metall. Sect. B-Metall. 48 B (2012) 461–469.
[2] H. Guler, R. Ertan, R. Ozcan, Mater. Sci. Eng. A 578 (2013) 417–421.
[3] S. Ojha, N.S. Mishra, B.K. Jha, Effect of cooling rate on the microstructure and mechanical properties of a C-Mn-Cr-B steel, Bull. Mater. Sci. 38 (2015) 531–536.
[4] T. Brune, D. Senk, R. Walpot, B. Steenken, Hot ductility behavior of boron containing microalloyed steels with varying manganese contents, Metall. Mater. Trans. B: Process Metall. Mater. Process. Sci. 46 (2015) 1400–1408.
[5] L.F. Kiss, T. Kemény, J. Bednarčík, J. Kamarád, Z. Arnold, Z. Konôpková, H.-P. Liermann, Pressure dependence of magnetic properties in Fe-Mn-B amorphous alloys: evidence for inhomogeneous ferromagnetism, J. Phys. Condens. Matter 25 (2013) (Article number 346002).
[6] G.F. Wang, H.L. Li, X.F. Zhang, Q. Ma, Y.L. Liu, Y.F. Li, Z.R. Zhao, Large magnetocaloric effect in Fe-B-Mn-Zr-Nb amorphous alloys near room temperature,

J. Supercond. Nov. Magn. 29 (2016) 1837–1842.
[7] M.I. Pashechko, Wear resistance of eutectic coatings of the Fe-Mn-C-B system alloyed with Si, Ni, and Cr, Mater. Sci. 46 (2011) 695–701.
[8] Z. Liu, Y. Li, X. Chen, K. Hu, Microstructure and mechanical properties of high boron white cast iron, Mater. Sci. Eng. A 486 (2008) 112–116.
[9] I. Smid, P. Rogl, F. Weitzer, The thernary system: manganese-boron-nitrogen, in: Proceedings of the 12th International Plansee Seminar '89: High Temperature and Wear Resistant Materials in a World of Changing Technology, May 8th to 12th, 1989, Reutte, Tirol, Austria, 4, 1990, pp. 577–598
[10] Y.B. Kuzma, M.V. Chepiga, A.M. Plakhina, Inorg. Mater. 2 (1966) 1220–1221.
[11] G. Pradelli, C. Gianoglio, Sul sistema ferro-manganese-boro, Metall. Ital. 68 (1976) 19–23.
[12] V.T. Witusiewicz, Thermodynamics of binary and ternary melts of the 3d transition metals (Cr, Mn, Fe, Co and Ni) with boron, Thermochim. Acta 264 (1995) 41–58.
[13] J. Miettinen, K. Lilova, G. Vassilev, Thermodynamic description of ternary Fe-B-X systems. Part 3: Fe-B-Mn, Arch. Metall. Mater. 59 (2014) 1481–1485.
[14] M. Hillert, L.-I. Staffansson, The regular solution model for stoichiometric phases and ionic melts, Acta Chem. Scand. 24 (1970) 3618–3626.
[15] V. Homolová, A. Kroupa, A. Výrostková, Calculation of Fe-B-V ternary phase diagram, J. Alloy. Compd. 520 (2012) 30–35.
[16] C. Guo, P.M. Kelly, Boron solubility in Fe-Cr-B cast irons, Mater. Sci. Eng. A 352 (2003) 40–45.
[17] O. Redlich, A. Kister, Thermodynamics of nonelectrolyte solutions -x-y-t relations in a binary system, Ind. Eng. Chem. 40 (1948) 341–345.
[18] M. Hillert, M. Jarl, A model for alloying in ferromagnetic metals, Calphad 2 (1978) 227–238.
[19] ⟨http://www.thermocalc.com/⟩
[20] T. Van Rompaey, K.C. Kumar Hari, P. Wollants, Thermodynamic optimization of the B-Fe system, J. Alloy. Compd. 334 (2002) 173–181.
[21] W. Sun, Y. Du, S. Liu, B. Huang, Ch Jiang, Thermodynamic assessment of Mn-B system, J. Ph. Equilib. Diffus. 31 (2010) 4.
[22] A. Kroupa, STEEL16 Database, 2010.
[23] A.T. Dinsdale, SGTE data for pure elements, Calphad 15 (1991) 317–425.
[24] L.E. Tergenius, Refinement of the crystal structure of orthorhombic Mn_2B (formerly denoted Mn_4B), J. Less-Common Met. 82 (1981) 335–340.
[25] P.K. Liao, K.E. Spear, The B-Mn (boron-manganese) system, Bull. Alloy Ph. Diagr. 7 (1986) 585–586.
[26] P. Villars, Pearson's Handbook, The Materials Information Society, Materials Park OH, 1997.